Calculation of strength, rigidity, and stability of the aircraft fuselage frame made of composite materials

Sergei I. IVANNIKOV*,[1], Yana A. VAHTEROVA[1], Yuri A. UTKIN[2], Ying SUN[3]

*Corresponding author
[1]Department of Resistance of Materials Dynamics and Strength of Machines,
Moscow Aviation Institute (National Research University),
4 Volokolamskoe Shosse, 125993, Moscow, Russian Federation,
sjivannikov@mail.ru*, yana-vahterova@mail.ru
[2]Department of Engineering Graphics,
Moscow Aviation Institute (National Research University),
4 Volokolamskoe Shosse, 125993, Moscow, Russian Federation,
uraalut@mail.ru
[3]Department of Mechanical Engineering, Hangzhou Xiaoshan Technician College,
448 Tonghui South Road, 311200, Xiaoshan District, Hangzhou Zhejiang, People's Republic of China,
695792773@qq.com

DOI: 10.13111/2066-8201.2021.13.S.8

Received: 10 March 2021/ Accepted: 20 June 2021/ Published: August 2021

Abstract: *Carbon-carbon composite materials (CCCM) are characterized by high heat resistance and thermostability for which they, in most of their physical and mechanical characteristics, can be attributed to the most promising materials. Approximately 81% of all carbon-carbon composite materials are used for the manufacture of brake rotors for aircraft, 18% – in space rocket technology, and only 1% – for all other areas of application. This study discusses calculations of the strength, rigidity, and stability of a frame made of carbon-carbon composite materials. It is known that the strength of CCCM based on high-strength carbon fibers is higher than the strength of a composite material based on high-modulus carbon fibers obtained at various processing temperatures. The stress-strain behaviour (SSB) of the material is carried out. Among the special properties of CCCM are low porosity, low coefficient of thermal expansion, maintaining a stable structure and properties, as well as product dimensions.*

Key Words: *carbon-carbon composite materials, stress-strain state, finite element model, physical and mechanical parameters, composite materials.*

1. INTRODUCTION

One of the most important problems of creating modern aircraft structures is to reduce their weight while maintaining strength and rigidity. The development of radiation-resistant, heat-resistant, lightweight materials from CCCM allows increasing the efficiency of the use of structural elements of the frame type [1], [2], which are used in the design of modern aircraft. In terms of the strength, rigidity and heat resistance of materials, special attention of designers

is drawn to carbon-carbon composite materials [3], [4]. Such materials have the highest specific strength and rigidity up to temperatures of 2800°C [5], high heat resistance, impact resistance, corrosion resistance, resistance to radiation exposure and low-temperature coefficients of linear expansion [6], [7]. The use of CCCMs in the hot-end components of modern aviation equipment reduces the weight of the structure [8], [9]. To create promising support frames, trusses, it is necessary to make strength calculations and confirm them experimentally. The mechanical strength of solids is determined by the strength of the interatomic bond [10], [11]. Of the natural bodies, diamond has the highest hardness, in which there are carbon-carbon interatomic bonds. Carbon-carbon bonds are also present in graphite [12]; it has a layered structure [13]. There are strong carbon-carbon bonds inside the layers. These bonds are used to create high strength materials. One of the important problems of creating designs of aviation, aircraft and rocket engines is the development of new materials used for the manufacture of the most loaded parts operating under high temperatures [14].

Various methods of studying materials with complex properties are described in researches of Y. Duan et al. [15], A. V. Babaytsev and L. N. Rabinskiy [16], L. N. Rabinskiy and O. V. Tushavina [17], N. A. Bulychev et al. [18], V. A. Zagovorchev and O. V. Tushavina [19], [20], M. Sha et al. [21], P. F. Pronina et al. [22], E. L. Kuznetsova et al. [23]. This study provides calculations for strength, stiffness, and deformation.

2. METHODS

The cowling is a mesh cylindrical shell formed by a system of spiral, annular and longitudinal ribs made by winding from a carbon fibre impregnated with a binder mesh shell, four access windows of a trapezoidal shape are provided. At the ends of the scowling, there are docking frames [24], [25]. The structure of the side frames is formed by alternating layers of carbon fibre composite based on a unidirectional carbon tape impregnated with a binder, and tapes of unidirectional material forming a system of grid shells. The height of the side frames – 65 mm, the thickness – 25 mm. The general view of the prototype frame is shown in Figure 1.

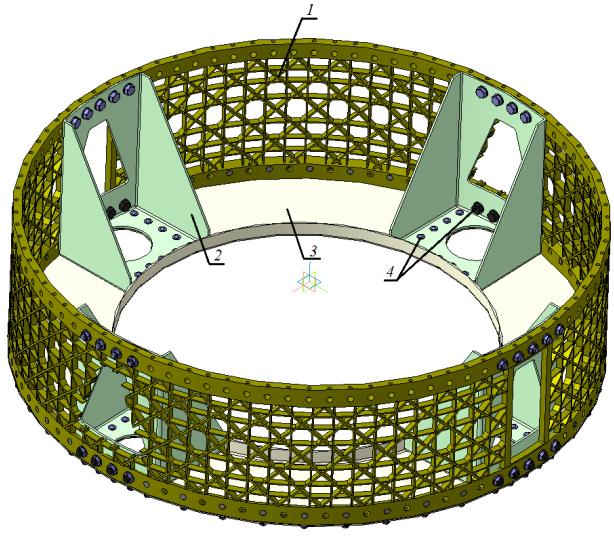

Fig. 1 – General view of the prototype frame

The prototype frame consists of cowling – 1, crossbars – 2, base – 3, and fasteners – 4. The frame structure includes 2 molded crossbars.

The thickness of the crossbar – 7 mm. The crossbar is attached to the grid shell by an adhesive joint.

The crossbar is fixed to the cowling by a bolted connection 4, to the base of the frame – by a rivet connection. Base 3 is made by molding from epoxy prepreg [26], [27].

The thickness of the base – 4 mm. Four holes with a diameter of 180 mm are cut in the base of the frame.

A collar with a height of 46 mm and a thickness of 4 mm is formed along the inner radius of the base. The attachment of base 3 to the cowling is carried out by means of a glue-mechanical connection.

3. RESULTS

The prototype frame is subject to the axial compressive forces $T_{cf} = 10000$ kgf, evenly distributed over the sites, in accordance with the load distribution shown in Figure 2.

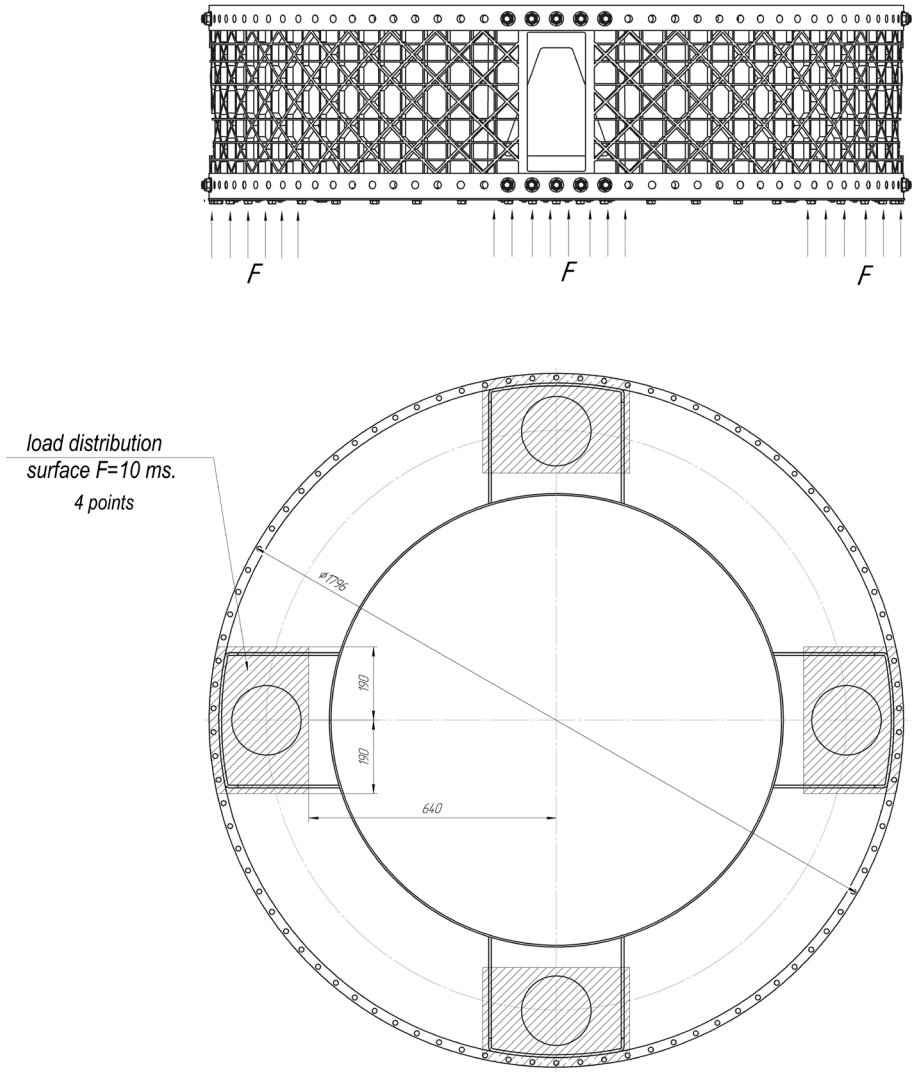

Fig. 2 – Load distribution

Stress-strain behaviour of the materials used in the design of the prototype frame. The stress-strain behaviour of the frame construction materials is given in Tables 1-3.

Table 1 – Stress-strain behaviour of carbon-fibre composite

Ser. No.	Parameter description	Value
1	Tensile strength in the direction of reinforcement σ_1, MPa (kgf/mm^2)	1205 (123)
2	Modulus of elasticity in the direction of reinforcement E_1, hPa (kgf/mm^2)	141.8 (14450)
3	Modulus of elasticity in the transversal direction E_2, hPa (kgf/mm^2)	5.97 (609)
4	Compressive strength in the direction of reinforcement σ_{-1}, MPa (kgf/mm^2)	533 (54.3)
5	Shear modulus in the reinforcement plane G, HPa (kgf/mm^2)	4.89 (498)
6	Poisson's ratio μ_{12}	0.29

Table 2 – Stress-strain behaviour of carbon-fibre composite based on unidirectional carbon tape impregnated with a binder

Ser. No.	Parameter description	Value
1	Tensile strength in the direction of reinforcement σ_1, MPa (kgf/mm^2)	1032 (105.2)
2	Modulus of elasticity in the direction of reinforcement E_1, hPa (kgf/mm^2)	120 (12250)
3	Modulus of elasticity in the transversal direction E_2, hPa (kgf/mm^2)	9.86 (1005)
4	Compressive strength in the direction of reinforcement σ_{-1}, MPa (kgf/mm^2)	461 (47.0)
5	Shear modulus in the reinforcement plane G, HPa (kgf/mm^2)	3.92 (400)
6	Poisson's ratio μ_{12}	0.145

Table 3 – Stress-strain behaviour of carbon-fibre composite based on epoxy prepreg

Ser. No.	Parameter description	Value	
		part "Base"	part "Crossbar"
1	Breaking tensile stress along the base σ_1, MPa (kgf/mm^2)	561 (57.2)	540 (55.0)
2	Breaking tensile stress along the weft σ_2, MPa (kgf/mm^2)	458 (46.7)	319 (32.5)
3	Modulus of elasticity along the base E_1, HPa (kgf/mm^2)	54.9 (5596)	64.1 (6534)
4	Modulus of elasticity along the weft E_2, HPa (kgf/mm^2)	50.7 (5168)	65.2 (6646)
5	Breaking tensile stress during compression along the base σ_{-1}, MPa (kgf/mm^2)	567 (57.7)	622 (63.4)
6	Breaking tensile stress during compression along the weft σ_{-2}, MPa (kgf/mm^2)	500 (51.0)	500 (51.0)
7	Shear modulus in the reinforcement plane G, HPa (kgf/mm^2)	10.7 (1091)	4.36 (444)
8	Poisson's ratio when stretched along the baseμ_{12}	0.23	0.15
9	Poisson's ratio at tension along the weft μ_{21}	0.12	0.12
10	Breaking tensile stress in shear in the reinforcement plane τ_{sh}, MPa (kgf/mm^2)	336 (34.3)	218 (22.2)

Calculation of the stress-strain behaviour (SSB) of a prototype frame by the finite element method. The general view of the finite element model (FEM) is shown in Figure 3.

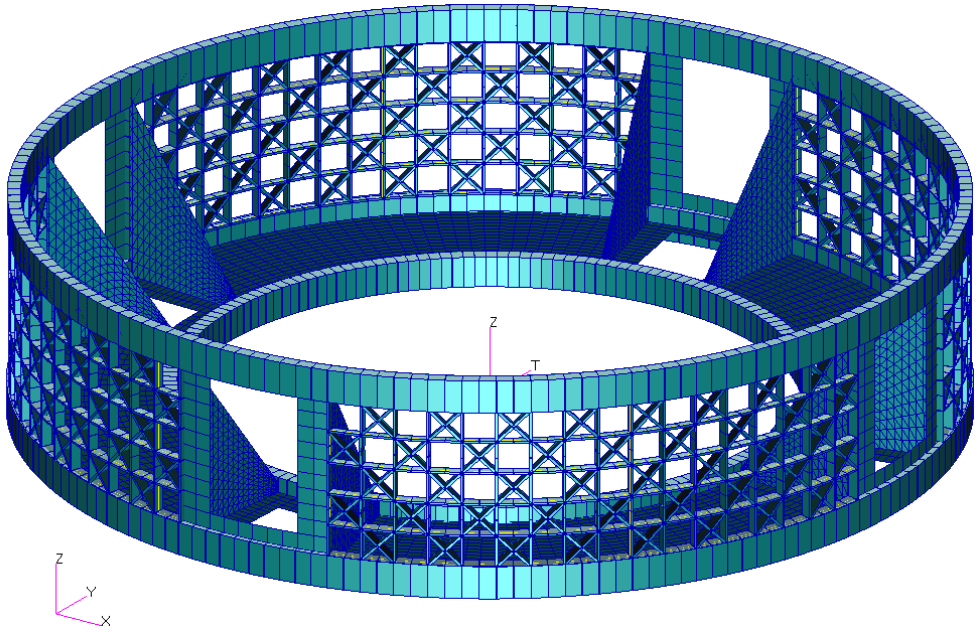

Fig. 3 – General view of the FEM

The FEM includes:

- beam end elements that model a system of spiral, annular, and longitudinal ribs of a mesh structure, cowling frames, and the base collar.
- three-node end elements that model the side shelves of crossbars;
- four-node end elements modelling the mold base, vertical and horizontal parts of crossbars.

The nature of the loading of the FEM is shown in Figure 4.

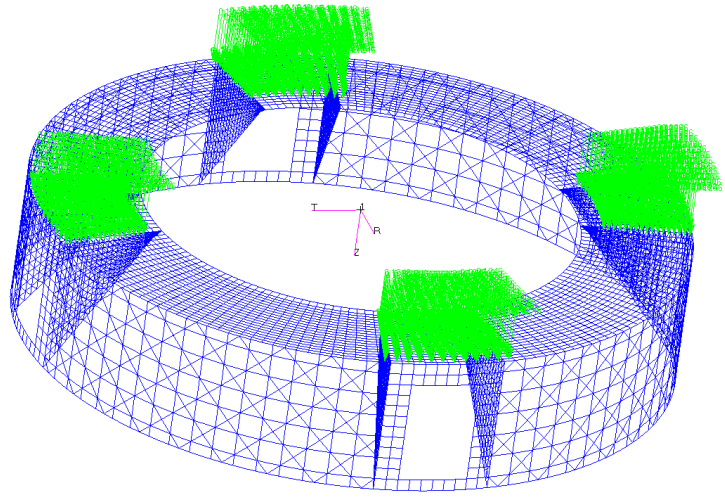

Fig. 4 – Loading scheme of the FEM of prototype frame ($T_{cf} = 40000$ kgf)

The maximum shear stresses in the reinforcement plane of crossbars and base are shown in Table 4.

Table 4 – Maximum shear stresses in the reinforcement plane

Construction element	Maximum shear stress τ_{sh}, kgf/mm^2	Safety margin for shear stresses η_τ
Crossbar (side walls)	4.85	4.6
Crossbar (horizontal section)	0.01	>10
Crossbar (back)	2.06	>10
Base	10.9	3.2

The nature of the distribution of normal stresses in beam elements simulating ribs and side frames is illustrated in Figure 5.

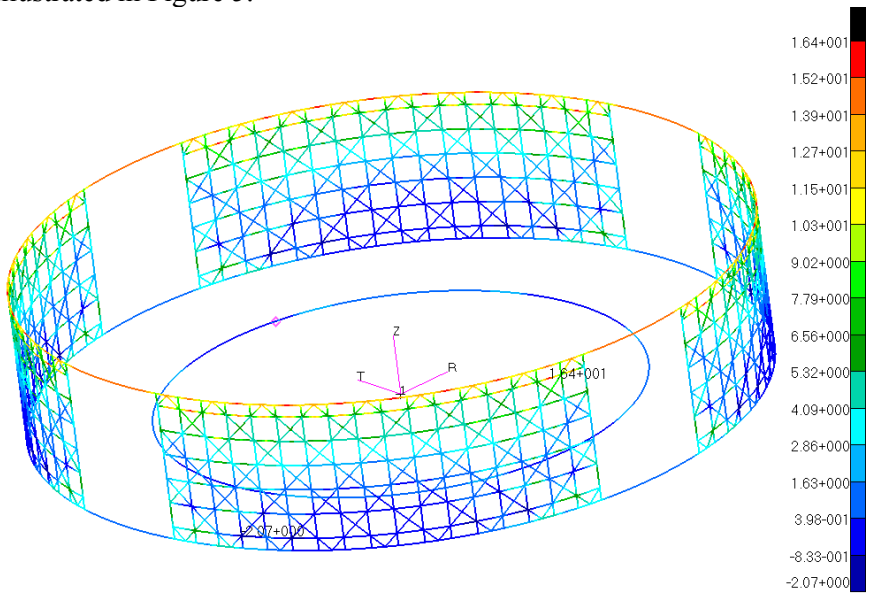

Fig. 5 – The nature of the distribution of normal stresses (kgf/mm^2) in the ribs and side frames of the prototype frame

To resist internal stresses generated by the combined effect of temperature gradient and disruption toads, a carbon-carbon composite limiter must, in general, also possess adequate compressive, flexural, and shear strengths. The latter two of these properties can be met with reasonable confidence.

However, carbon-carbon composites do not generally behave well under compressive stress [28], [29].

This problem is compounded with the trend for lower fiber strength to be coupled with higher modulus and degree of crystallinity [30], [31].

These high-modulus fibers are precisely the ones that are desirable if the coefficient of thermal expansion is to be reduced in the x-y plane.

Furthermore, it should be remembered that electrical resistivity will decrease with increased fiber crystallinity.

The nature of the stress distribution in the three- and four-node elements that model crossbars and base is illustrated in Figure 6.

Here, the stresses in the direction of the base of the material are shown for the base, back, and side walls of the crossbar.

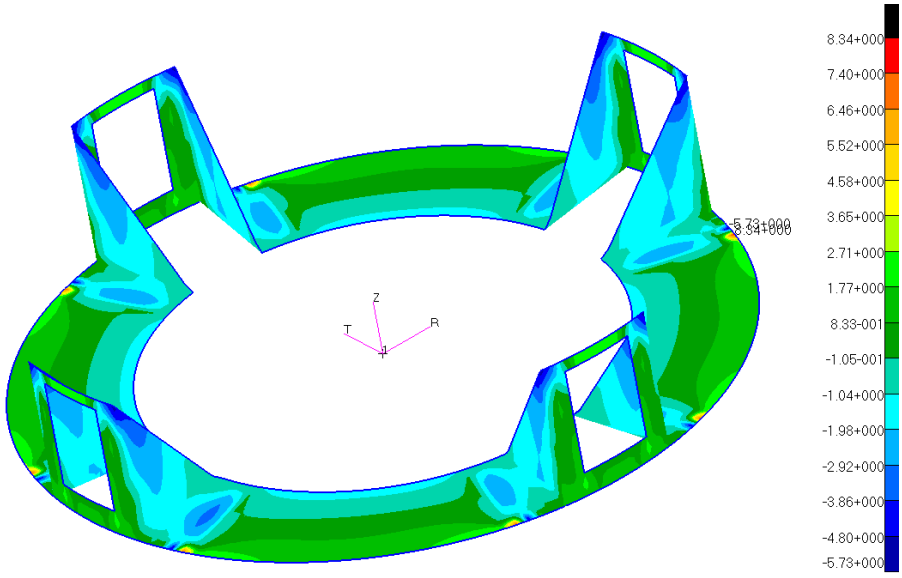

Fig. 6 – The nature of the stress distribution (kgf/mm^2) in crossbars and base

Figure 7 shows the deformed state of the prototype frame from a given load. The blue colour shows the FEM in its original state, and the black colour shows the deformed model. The maximum axial movement of the frame $w = 2.47$ mm.

Knowing the axial movement of the prototype frame from a given load, the rigidity of the structure can be determined by the equation:

$$K = \frac{T}{w} \tag{1}$$

$$K = \frac{40000}{2.47} = 16194.3 \text{ kgf/mm} \tag{2}$$

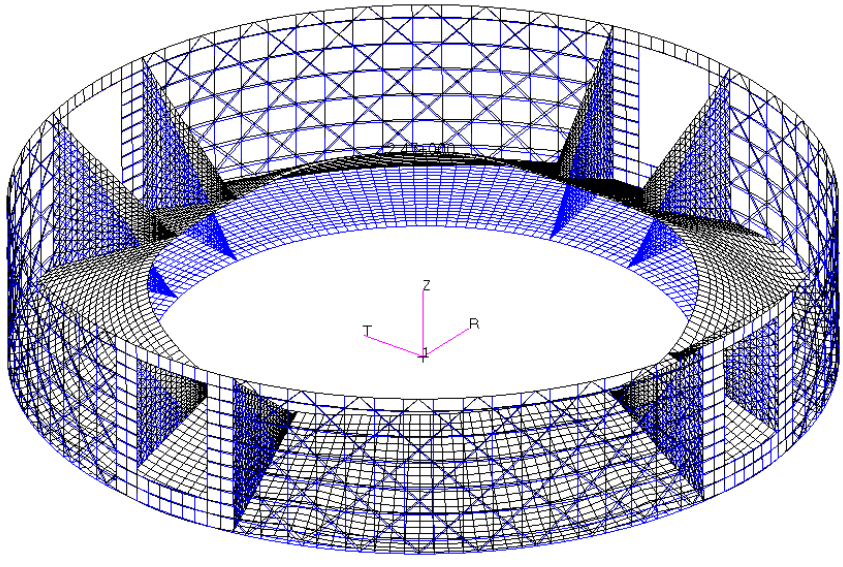

Fig. 7 – Deformed state of the prototype frame

As a result of calculating the stability of the prototype frame from the action of the axial load $T_{cf} = 40000$ kgf, a critical load value equal to $T_{cr} = 192000$ kgf was obtained.

The stability margin is determined by the equation

$$\eta_{st} = \frac{T_{cr}}{T_{cf}} = \frac{192000}{40000} = 4.8 \tag{3}$$

The buckling mode is illustrated in Figure 8. The blue colour in the figure shows the FEM in its initial state, and the black colour shows it after the loss of stability.

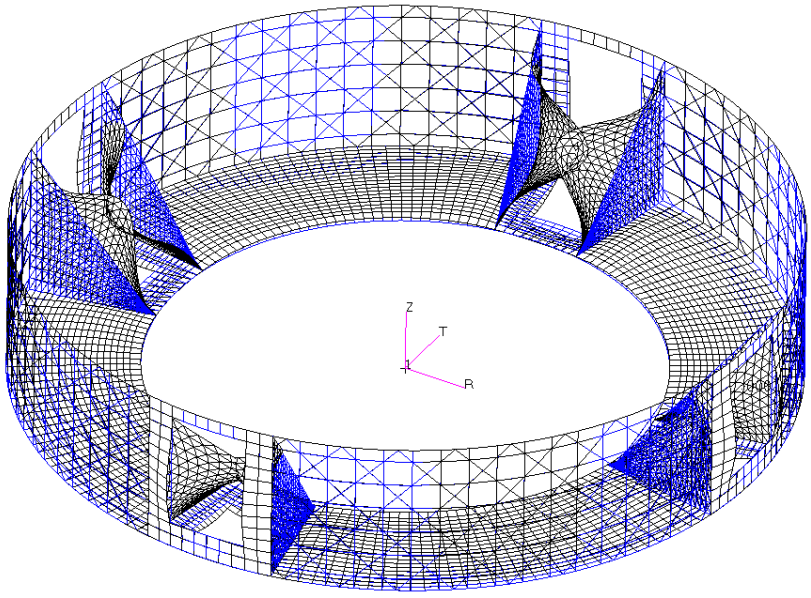

Fig. 8 – The buckling mode

The rigidity of the cowling of the prototype frame from the axial compressive force $T_{cf} = 40000$tf, acting on the structure evenly, calculated by the equation

$$EF = \frac{TL}{w_1} = \frac{40000 \cdot 500}{0{,}23} = 0{,}87 \cdot 10^8 \text{kgf} \tag{4}$$

where $L = 500$ mm – length of the cowling; $w_1 = 0{,}23$ mm – maximum displacement of the cowling in the axial direction.

4. CONCLUSIONS

The calculation performed in the paper confirmed the operability of the prototype frame design at the specified operating loads. The necessity of using beam finite elements simulating a system of spiral, annular, and longitudinal edges of a mesh structure is also confirmed by this study. It is important to note that for the side shelves of the crossbar, it is convenient to use three-node end elements, and for the mold base of the vertical and horizontal part of the traverse, four-node end elements. For the deformed state, displacement plots are calculated, showing an adequate coincidence of theoretical evaluation and approximate solutions. The forms of the stability loss correspond to the deformation pattern.

ACKNOWLEDGEMENTS

The work was carried out with the financial support of the state project of the Ministry Science and Higher Education of the Russian Federation "Theoretical and experimental research in production and processing of advanced metal and composite materials based on aluminum and titanium alloys", project No. FSFF-2020-0017.

REFERENCES

[1] E. L. Kuznetsova and L. N. Rabinskiy, Linearization of radiant heat fluxes in the mathematical modeling of growing bodies by the action of high temperatures in additive manufacturing, *Asia Life Sciences*, no. **2**, pp. 943-954, 2019.

[2] A. V. Makarenko and E. L. Kuznetsova, Energy-efficient actuator for the control system of promising vehicles, *Russian Engineering Research*, vol. **39**, no. 9, pp. 776-779, 2019.

[3] E. L. Kuznetsova and L. N. Rabinskiy, Numerical modeling and software for determining the static and linkage parameters of growing bodies in the process of non-stationary additive heat and mass transfer, *Periodico Tche Quimica*, vol. **16**, no. 33, pp. 472-479, 2019.

[4] V. F. Formalev, S. A. Kolesnik and E. L. Kuznetsova, Analytical study on heat transfer in anisotropic space with thermal conductivity tensor components depending on temperature, *Periodico Tche Quimica*, vol. **15** (Special Issue 1), pp. 426-432, 2018.

[5] N. A. Bulychev and L. N. Rabinskiy. Ceramic nanostructures obtained by acoustoplasma technique, nanoscience and technology, *An International Journal*, vol. **10**, no. 3, pp. 279-286, 2019.

[6] A. N. Danilin, L. N. Rabinskiy and S. I. Zhavoronok, Deformation of the helical type wire structures, *Periodico Tche Quimica*, vol. **16**, no. 33, pp. 583-601, 2019.

[7] V. F. Formalev, S. A. Kolesnik, and E. L. Kuznetsova, Approximate analytical solution of the problem of conjugate heat transfer between the boundary layer and the anisotropic strip, *Periodico Tche Quimica*, vol. **16**, no. 32, pp. 572-582, 2019.

[8] N. A. Bulychev and L. N. Rabinskiy, Ceramic nanostructures obtained by acoustoplasma technique, *Nanoscience and Technology: An International Journal*, vol. **10,** no. 3, pp. 279-286, 2019. https://doi.org/10.1615/NanoSciTechnolIntJ.2019031161

[9] A. V. Babaytsev and A. A. Zotov, Designing and calculation of extruded sections of an inhomogeneous composition, *Russian Metallurgy (Metally),* no. **13**, pp. 1452-1455, 2019.

[10] A. A. Orekhov, Yu. A. Utkin and P. F. Pronina, Determination of deformation in mesh composite structure under the action of compressive loads, *Periodico Tche Quimica*, vol. **17**, no. 35, pp. 599-608, 2020.

[11] A. V. Babaytsev, A. A. Orekhov and L. N. Rabinskiy, Properties and microstructure of AlSi10Mg samples obtained by selective laser melting, *Nanoscience and Technology: An International Journal*, vol. **11**, no. 3, pp. 213-222, 2020.

[12] O. V. Egorova, A. S. Kurbatov, L. N. Rabinskiy and S. I. Zhavoronok, Modeling of the dynamics of plane functionally graded waveguides based on the different formulations of the plate theory of I.N. Vekua type, *Mechanics of Advanced Materials and Structures*, vol. **28**, no. 5, pp. 506-51, 2021.

[13] V. A. Pogodin, A. N. Astapov and L. N. Rabinskiy, CCCM specific surface estimation in process of low-temperature oxidation, *Periodico Tche Quimica*, vol. **17**, no. 34, pp. 793-802, 2020.

[14] E. L. Kuznetsova and L. N. Rabinskiy, Modeling the effects of buckling arising in production of thin-walled parts using selective laser melting (SLM) technology, *Asia Life Sciences*, no. **1**, pp. 601-611, 2019.

[15] Y. Duan, Z. Liu, X. Zhao, N. Hou, B. Du, H. Liu, Z. Zhao, B. Hou, Y. Li and L. N. Rabinskiy, Crushing behavior of honeycomb vs. foam under combined shear-compression loading, *International Journal of Impact Engineering*, no. **146**, 103696, 2020.

[16] A. V. Babaytsev and L. N. Rabinskiy, Design calculation technique for thick-walled composite constructions operating under high-speed loading, *Periodico Tche Quimica*, vol. **16**, no. 33, pp. 480-489, 2019.

[17] L. N. Rabinskiy and O. V. Tushavina, Investigation of an elastic curvilinear cylindrical shell in the shape of a parabolic cylinder, taking into account thermal effects during laser sintering, *Asia Life Sciences*, no. **2**, pp. 977-991, 2019.

[18] N. A. Bulychev, L. N. Rabinskiy and O.V. Tushavina, Effect of intense mechanical vibration of ultrasonic frequency on thermal unstable low-temperature plasma, *Nanoscience and Technology: An International Journal*, vol. **11**, no. 1, pp. 15–21, 2020.

[19] V. A. Zagovorchev and O. V. Tushavina, Selection of temperature and power parameters for multi-modular lunar jet penetrator. *INCAS Bulletin*, vol. **11**, pp. 231-241, https://doi.org/10.13111/2066-8201.2019.11.S.23, 2019.
[20] V. A. Zagovorchev and O. V. Tushavina, The use of jet penetrators for movement in the lunar soil, *INCAS Bulletin*, vol. **11**, pp. 221-230, https://doi.org/10.13111/2066-8201.2019.11.S.22, 2019.
[21] M. Sha, Yu. A. Utkin, O. V. Tushavina and P. F. Pronina, Experimental studies of heat and mass transfer from tip models made of carbon-carbon composite material (CCMM) under conditions of high-intensivity thermal load, *Periodico Tche Quimica*, vol. **17**, no. 35, pp. 988-997, 2020.
[22] P. F. Pronina, O. V. Tushavina and E. I. Starovoitov, Study of the radiation situation in Moscow by investigating elastoplastic bodies in a neutron flux taking into account thermal effects, *Periodico Tche Quimica*, vol. **17**, no. 35, pp. 753-764, 2020.
[23] E. L. Kuznetsova and A. V. Makarenko, Mathematic simulation of energy-efficient power supply sources for mechatronic modules of promising mobile objects, *Periodico Tche Quimica*, vol. **15**(Special Issue 1), pp. 330-338, 2018.
[24] A. A. Skvortsov, D. E. Pshonkin and M. N. Luk'yanov, Influence of constant magnetic fields on defect formation under conditions of heat shock in surface layers of silicon. *Key Engineering Materials*, vol. **771**, pp. 124-129, 2018.
[25] V. V. Ryndin, Mathematical modeling of the process of filling an engine through an inlet manifold, *Izvestia Vyssih Ucebnyh Zavedenij. Masinostroenie,* vol. **2**, pp. 71-75, 1980.
[26] V. I. Ivin and V. V. Ryndin, Unsteady flow in branched ducts of inlet pipes of internal combustion engines, *Izvestia Vyssih Ucebnyh Zavedenij. Masinostroenie,* vol. **9**, pp. 100-105, 1976.
[27] V. P. Privalko, R. V. Dinzhos, N. A. Rekhteta and F. J. B. Calleja, Structure-diamagnetic susceptibility correlations in regular alternating terpolymers of ethene and propene with carbon monoxide, *Journal of Macromolecular Science – Physics,* vol. **42B**, no. 5, pp. 929-938, 2003.
[28] R. V. Dinzhos, N. M. Fialko and E. A. Lysenkov, Analysis of the thermal conductivity of polymer nanocomposites filled with carbonnanotubes and carbon black, *Journal of Nano- and Electronic Physics,* vol. **6**, no. 1, 01015, 2014.
[29] A. N. Alekseev, S. A. Alekseev, Y. F. Zabashta, K. I. Hnatiuk, R. V. Dinzhos, M. M. Lazarenko, Y. E. Grabovskii and L. A. Bulavin, Two-dimensional ordered crystal structure formed by chain molecules in the pores of solid matrix, *Springer Proceedings in Physics,* vol. **221**, pp. 387-395, 2019.
[30] A. Beljatynskij, O. Prentkovskis and J. Krivenko, The experimental study of shallow flows of liquid on the airport runways and automobile roads, *Transport,* vol. **25**, no. 4, pp. 394-402, 2010.
[31] H. Yuilin, A. Beljatynskij and A. Ishchenko, Non-Roundabout design of cancel the intersection signal light on horizontal plane, *E3S Web of Conferences,* vol. **91**, 05003, 2019.